C.P. No. 697

C.P. No. 697

MINISTRY OF AVIATION

AERONAUTICAL RESEARCH COUNCIL

CURRENT PAPERS

Two-Dimensional Separated or Cavitating Flow Past a Flat Plate Normal to the Stream

By

G.E. Gadd, Ph.D., Ship Division, N.P.L.

LONDON: HER MAJESTY'S STATIONERY OFFICE

1963

SIX SHILLINGS NET

TWO-DIMENSIONAL SEPARATED OR CAVITATING FLOW PAST A FLAT PLATE NORMAL TO THE STREAM

by

C.P. No. 697
November, 1962

G. E. Gadd

Ship Division, National Physical Laboratory

SUMMARY

The applicability of inviscid-flow models to non-cavitating or cavitating flow past a normal plate is discussed. A new inviscid model is developed, with the aim of predicting features such as cavity length better than previous models. Experiments on air flow past a plate are described and the results compared with those of the theory. Finally the few experimental results available for cavitating flow are discussed.

Replaces Ship Division Report No. 38 - A.R.C. 24,247.

1. INTRODUCTION

The two-dimensional flow past a normal flat plate is perhaps the simplest bluff-body flow, being symmetrical and having fixed separation points. In itself this flow is of little practical interest, since few aero- or hydrodynamical devices have parts consisting of flat plates broadside to the stream. However it is useful to try and obtain a thorough understanding of the flat-plate flow, to throw light both on industrial aerodynamic problems, such as wind loads on chimney stacks, and also on cavitating liquid flows, such as occur with fully cavitating hydrofoils or propellers.

The flow past a flat plate with cavitation is not radically different from that without, because in both cases the pressure is roughly constant for some distance downstream of the plate along the mean-flow streamlines, such CD in Fig.1, passing through the edges of the plate. This constant pressure is usually close to the vapour pressure, the lowest pressure achieved anywhere in the flow field, when cavitation occurs, though with non-cavitating flow the pressure on the centre line of the wake just downstream of the plate can be much lower than that along CD. In either case, however, along the streamline through C, the pressure downstream of the initial constant-pressure portion CD rises till it reaches the free-stream value far downstream.

In non-cavitating flow the average pressure along CD, and correspondingly the drag coefficient, are not known a priori. Therefore if they could be predicted theoretically it would advance our understanding of the problem, as it would also if we could fully account for the fluctuating features of the flow. The fluctuations, involving unsteady force components on the body, are associated with the periodic shedding of vortices to form something like a Karman vortex street in the wake, though at the higher Reynolds numbers these vortices are turbulent and the shedding is not perfectly regular. These unsteady effects occur when the oncoming stream itself is steady, but it would also be useful to find out what happens when the oncoming stream is gusty, unsteady in speed and direction, like the natural wind.

In cavitating flow with extensive vaporous cavitation, the cavity pressure is known a priori, being almost equal to the vapour pressure, and hence the drag coefficient is also approximately known. The streamwise extent of the cavity, however, is not known, and it would be useful to understand what determines its position of closure. This is because hydrodynamical devices involving flow cavities are unlikely to operate successfully unless the cavities terminate well downstream of their solid surfaces. If this condition is not met, serious buffeting will probably occur, somewhat similar to the compressibility buffet an aircraft may experience at transonic speeds. Cavitation buffet arises from the unsteady processes of entrainment at the downstream ends of cavities. These processes are probably related to the tendency, mentioned above, for unsteady vortex shedding to occur behind a bluff body. A detailed understanding of them, however, can probably only be gained with the help of experiments.

The present paper describes contributions towards solving some of the above problems. The extent to which steady, inviscid-flow models are applicable to the real flows is discussed. A new inviscid model is developed, with the aim of predicting features such as cavity length better than previous models. Experiments on air flow past a flat plate are described, and the results compared with those of the theory. It is intended also to investigate experimentally cavitating water flows past a plate: these experiments will, it is hoped, form the subject of a later paper.

2. THE APPLICABILITY OF INVISCID-FLOW MODELS

In the real flow past a flat plate, the mean-flow streamlines through the plate edges must, as shown in Fig. 1, return to the axis of symmetry downstream. If, however, one were to calculate the inviscid flow past the boundary ABCDEF of Fig. 1, it would probably not be very similar to the real flow because in reality frictional effects are important along and near DEF. However, it may be possible to obtain a fair representation of the real flow if, in the inviscid-flow model, the streamlines springing from the plate edges are such that the pressure is constant along them for some distance downstream of the plate, and if they meet certain other conditions discussed below. These streamlines through the plate edges are called "free streamlines" because their shape is initially unknown, and part of the mathematical problem is to find it. This approach is an extension of the classical Kirchoff solution, in which the pressure everywhere along the free streamlines is postulated to be constant, equal to the pressure in the undisturbed stream.

As was pointed out above, the real flow is not steady, even when the oncoming stream is, because in non-cavitating flow there is something like a vortex street in the wake, and this is also probably true downstream of the cavity in cavitating flow.[1] Fig. 2 shows the real flow schematically.

The vorticity centres indicated are continually being generated behind the plate in air flow and behind the cavity in cavitating liquid flow. They move downstream relative to the plate at less than the free-stream velocity. The lines CF, C'F' represent the limits of frictional effects, Bernouilli's equation being satisfied outside of them, whereas inside there is a loss of total head. The flow between CF and C'F' is, at least over the downstream regions, subject to large, quasi-periodic fluctuations, and there may perhaps be appreciable fluctuations outside of CF and C'F'. Define coordinates x and y as in Fig. 2, with the origin at B, the centre of the face of the plate. Suppose the separation t between lines CDE, C'D'E' is equal to the wake displacement thickness δ^*_W, given by $\int_{-ye}^{ye}\left(1 - \frac{\rho u}{\rho_e u_e}\right)dy$. Here suffix e denotes conditions at the edge of the region of frictional effects, (i.e. along CF, C'F'), and ρ is the time-mean density, constant everywhere in incompressible air flow, and in the liquid-phase region of liquid flow, but virtually zero within a vaporous cavity. Further, u is the time-mean x-component of velocity, and the integration is carried out at constant x. Then we may hope that if we could calculate the steady inviscid flow over the boundary ABCDE, so defined, it would resemble, roughly at any rate, the time mean of the actual flow outside the frictional wake region.

The above assumption may be justified by the following considerations. The entrainment angle between the mean-flow streamlines and CF is likely to be quite small near C, so that since the inclination of CF to the x axis is large here, the streamline direction will be approximately that of CF. But close behind the plate, u will be very small, so that $\delta^*_W \approx 2y_e$, and the directions of CD and CF will be virtually the same. (For cavitating flows indeed CF will probably coincide with CD for a considerable distance.) Thus the inviscid model will have approximately the correct streamline inclination near the edges of the plate. Furthermore, since the velocity returns to its free-stream value far downstream outside of the wake, continuity considerations show that here the streamlines in the inviscid model will be displaced outwards relative to their positions well upstream of the plate by the same amount as in the real flow. It is, however, arguable that if we are primarily interested in the flow fairly near the plate, the displacement condition downstream is of small importance.

When the problem was considered initially, it was hoped that it would be possible to find the flow past a boundary such as ABCDE, defined by a number of disposable parameters. It would be specified that the pressure must be constant along the initial portion CD of CDE, but in non-cavitating flow this pressure would be initially unknown. Likewise downstream it would be specified that $t = \delta^*_W \to \frac{1}{2}C_D\delta$, where C_D is the drag coefficient and δ the plate height CC': this condition follows from momentum considerations since the momentum thickness and displacment thickness of the wake become the same downstream. Other parameters would be left disposable, and it was hoped to be able to match the resulting pressure distribution along CDE to a boundary-layer type of solution for the wake. However the large fluctuations associated with the vortex-street type of formation, and the corresponding large pressure differences across the wake in the y-direction, make it impossible to perform this matching procedure at all accurately. The situation would be better for cases where the x axis is a solid boundary, namely for flows past spoilers, where the vortex street is large suppressed[2,3]. Since, however, practical industrial-aerodynamic or cavitating-flow cases usually involve free wakes, solutions for spoilers are perhaps of limited usefulness.

Although the matching procedure discussed above cannot be carried out accurately, it is still possible to improve on existing free-streamline theories in which the base or cavity pressure coefficient is the sole disposable parameter. For a given value of this parameter, the drag coefficient is predicted to be virtually the same by all the models, except for unrealistically high base suctions which no real flow could sustain. However the predicted cavity shapes vary widely. Thus Fig. 3 shows three different models for flow past a normal flat plate, drawn roughly to the same scale for a pressure coefficient $(p - p_0)/\frac{1}{2}\rho u_0^2$ of about -1.25 in the cavity. In the first model, due to Riabouchinsky[4], the flow re-attaches symmetrically to an artificial image plate introduced at the end of the cavity. The combination of the two plates has zero drag and the ultimate wake thickness is zero. The second model, that of the re-entrant jet, has been discussed by a number of workers. (See Ref. 5, where a bibliography is given). Here it is supposed that a jet of fluid passes upstream through the middle of the cavity and vanishes at the plate. This of course is an unreal feature, though it has some similarity to the spray often thrown forward inside real cavities. As in the Riabouchinsky model, there is a stagnation point behind the cavity. However in effect the downstream wake thickness is slightly negative: streamlines finish up nearer to the centre line downstream than they started upstream, due to the fluid removed in the re-entrant jet. The third case in Fig. 3 is sometimes called the wake-dissipation model, but is perhaps better described as the parallel-streamline model. It has been developed independently by several people, including Roshko[6] and Gerber and McNown[7]. Here the downstream wake thickness is not zero. The pressure is initially constant along the streamlines springing from the plate edges, until they become parallel to the axis of symmetry: from this point on the direction of the free streamlines remains constant and the pressure rises till it asymptotes downstream to the free-stream value. This feature of the model has been singled out by Birkhoff[8] as rendering it more applicable than the other two models to non-cavitating wakes. By implication the zero or effectively negative downstream wake thickness of these other models is presumably considered to be no disadvantage in applications to cavitating flows, and according to Ref. 9, several workers have attempted to find a model for cavitating flows with a cusped, closed cavity as in Fig. 4. The purpose of the cusp is to avoid the stagnation point of the Riabouchinsky or re-entrant jet models. However whilst the time-average streamlines passing through the edges of the plate in a real cavitating flow may perhaps, as sketched in Fig. 1, have a shape something like the cusped cavity of Fig. 4, the solution for the inviscid flow past such a boundary would differ considerably from the real flow, as was pointed out above. Just downstream of the cavity the process of entrainment of vapour from the cavity probably exerts a large retarding force on the liquid: this entrainment will be balanced by vaporisation from the liquid boundaries of the cavity nearer to the plate. Thus there is likely to be slow-moving liquid just behind the cavity and a far from zero displacement thickness in the shaded region of Fig. 4. The wake continues to be thick downstream, as is required by the momentum balance, which, as stated earlier, shows that downstream

$$\delta^*_W \to \tfrac{1}{2}C_D\delta \qquad \ldots (1)$$

Woods[10] has developed a free streamline model with a finite, non-zero, wake thickness downstream, in qualitative accordance with equation (1). However he made no attempt to satisfy that equation quantitatively, merely using the finite-thickness condition to narrow down the choice of analytically convenient specifications of the pressure on the downstream portions of the free streamlines.

Equation (1) is not strictly true for an inviscid vortex-street model of a wake, where the velocities are assumed not to asymptote to u_0 downstream. The vortex street is shown in Fig. 5. If the circulation of each vortex is κ, the average x-component velocity between the rows is $-\frac{\kappa}{a}$ relative to the fluid at infinity[11], whilst outside the rows it is zero. Hence the average value of δ^*_W is $\kappa h/au_0$, so according to equation (1) the drag D should be $\rho\kappa hu_0/a$. In fact

$$D = \frac{\rho\kappa h u_o}{a}\left(1 - \frac{2u_s}{u_o} + \frac{\kappa}{2\pi h u_o}\right)$$

where u_s is the velocity of the vortices in the street relative to the fluid at infinity. But for the stable configuration of trail $h = 0.281a$ and $\kappa = 2\sqrt{2}au_s$ so that

$$D = \frac{\rho\kappa h u_o}{a}\left(1 - 0.396\,\frac{u_s}{u_o}\right).$$

Since u_s/u_o is typically about $^1/_4$, D does not differ greatly from $\rho\kappa h u_o/a$. Hence the wake displacement thickness will not be seriously miscalculated by equation (1), even if vortex-street features are present in the wake.

These features can, however, give rise to considerably reduced pressures near the wake centre line as compared with the edge of the wake. The flow in an inviscid trail is steady with respect to axes moving with the vortices. Consider a point W, as in Fig. 5, midway between a vortex of one row and an adjacent one of the other row. Here, relative to the fluid at infinity, the x and y component velocities are both of magnitude κ/a. Relative to axes moving with the vortices, the component velocities at W are therefore of magnitudes $\frac{\kappa}{a}\left(1 - \frac{1}{2\sqrt{2}}\right)$ and κ/a, whilst outside the street the velocity is $\kappa/(2\sqrt{2}a)$. Hence if the pressure at W is p_w, Bernoulli's equation requires

$$p_w + \tfrac{1}{2}\rho\frac{\kappa^2}{a^2}\left[\left(1 - \frac{1}{2\sqrt{2}}\right)^2 + 1\right] = p_o + \tfrac{1}{2}\rho\,\frac{\kappa^2}{8a^2}$$

Hence the pressure coefficient

$$C_{pw} = \frac{p_w - p_o}{\frac{1}{2}\rho u_o^2} = -\frac{\kappa^2}{a^2 u_o^2}\left(2 - \frac{1}{\sqrt{2}}\right).$$

But $$C_D = \frac{D}{\frac{1}{2}\rho u_o^2 \delta} \approx \frac{2\kappa h}{a u_o \delta}$$

from the previous paragraph, so that

$$C_{pw} \approx -\frac{1}{4}\left(2 - \frac{1}{\sqrt{2}}\right)C_D{}^2 \ \frac{\delta^2}{h^2} \ .$$

For a flat plate, therefore, in non-cavitating flow with $C_D \approx 2$, $C_{pw} \approx -1.3\ \delta^2/h^2$. This can lead to a pressure coefficient in the middle of the wake of the order of -0.4, since the trail adjusts itself so that the lateral spacing h of the vortex rows is nearly twice the height δ of the plate generating the trail. This explains the low pressures measured on the centre line of the wake of a two-dimensional normal flat plate in the experiments of Refs. 2 and 12 and of Section 4 below.

All this means that no steady inviscid-flow model can hope to give an accurate time-average of the real flow over the complete field, including the wake. However, if free-streamline models are used with disposable parameters chosen so as to match the external flow, in a necessarily crude way, to the wake flow, then at least we may hope that they will indicate correctly the order of magnitude of the cavity length. No clear indication of this is provided by the existing models of Fig. 3, since the parallel-streamline model predicts a very much shorter cavity than the others, if we define the cavity as extending over the region of constant pressure. The next section therefore attempts to develop a more adequate model.

3. POSSIBLE NEW FREE-STREAMLINE MODELS

We expect to obtain some resemblance to the actual flow with a model in which t, the distance apart of the free streamlines, is equal to the wake displacement thickness δ^*_w. The value of t far downstream will thus, from equation (1), be approximately equal to the plate height δ for a flat plate in non-cavitating flow with C_D about 2. When there is an extensive cavity the base suction will be relatively less than in non-cavitating flow, and C_D will be less than 2. Thus then the downstream value of t will be less than δ. We therefore look for a model in which the free streamlines, after springing outwards from the plate edges, partially neck in, and then turn parallel to each other to form a wake of finite downstream thickness, equal to or less than the plate height δ.

Fig. 6 shows a representation in the so-called hodograph plane of a free-streamline model which can meet these conditions. The full line is the streamline ABCDE of Fig. 2 plotted in terms of the velocity components u and v The coordinates are u and $-v$, or $q \cos \theta$ and $-q \sin \theta$, where q is the fluid speed and θ is the streamline inclination to the x axis. Thus far upstream, at A, $u = u_0$ and $\theta = 0$. At the stagnation point B, $u = v = 0$, or $q = 0$, and along AB, $\theta = 0$. Along BC, $\theta = \frac{\pi}{2}$, the streamline angle abruptly changing from 0 to $\frac{\pi}{2}$ at B. At C and along CD the pressure is constant at some value below the pressure in the free stream, so $q = Nu_0$, where N is a constant greater than 1, and CD is part of a circle in the hodograph plane. Finally along DE the pressure returns to its free-stream value, i.e. q returns to u_0, and the flow angle θ returns to zero.

Other streamlines of the flow, outside of ABCDE in Fig. 2, would map in the hodograph plane to lines inside ABCDE, as indicated by the dotted line in Fig. 6. This method of representation forms the basis of the very old-established theory for free-streamline problems, whose principles are now recapitulated briefly as follows. The shape of the free streamlines is initially completely unknown in the physical plane of Fig. 2, but known for the portion CD in the hodograph plane: this, of course, is the reason for using the hodograph plane. Denote by z the complex coordinate $x + iy$ in the physical plane, by ν the complex coordinate $u - iv$ or $qe^{-i\theta}$ in the hodograph plane, and by w the complex potential $\phi + i\psi$, where ϕ is the potential function and ψ the stream function, zero, let us say, on ABCDE. Then it may be shown (as in Ref. 13) that ϕ and ψ satisfy Laplace's equation in the hodograph plane as well as in the physical plane. Thus $\partial^2\psi/\partial u^2 + \partial^2\psi/\partial v^2 = 0$, for example. This means that equipotentials and streamlines map in the hodograph plane as a grid of lines (curved in general) intersecting at right angles, and if they are plotted for vanishingly small equal increments of ϕ and ψ, the elements of the grid are squares. Moreover ϕ and ψ satisfy Laplace's equation in any equation derived from the hodograph plane by a process of conformal transformation since, by definition, in such a transformation the grid elements remain squares except at isolated singular points. Suppose, by a suitable sequence of transformations, that the line ABCDE of Fig. 6 can be mapped to a straight line, the real axis in a plane of complex coordinate ε, say. Then $w = J\varepsilon$, where J is a constant, satisfies Laplace's equation in this plane together with the boundary condition that the stream function ψ is zero on ABCDE. Hence by a process of inversion the flow may be found in the hodograph plane, and from this, in the physical plane, since

$$\frac{dw}{dz} = u - iv = \nu$$

so that

$$z = \int \frac{dw}{\nu} .$$

We now apply these principles to the case of Fig. 6, making the transformations shown in Fig. 7. To remove the right angle at B in Fig. 6 we square ν. In the ν^2 plane the coordinates of A,E are $(u_0^2, 0)$ and since all the flow at infinity crowds into this point we invert about it, i.e. map on to the plane of $(\nu^2 - u_0^2)^{-1}$. In the process of inversion a circle remains a circle, so that CD is still circular. Shifting the origin to the centre of the circular arc CD we obtain the λ plane, defined by

$$\lambda = \frac{1}{\nu^2 - u_0^2} - \frac{1}{(N^4 - 1)u_0^2} = \frac{N^4 u_0^2 - \nu^2}{(\nu^2 - u_0^2)(N^4 - 1)u_0^2} \qquad \ldots (2)$$

Applying the Joukowski transformation to this we transform to the plane of $\lambda + N^4/[(N^4-1)^2 u_0^4\lambda]$, in which the circular arc CD becomes a straight line. The point H on CD at which the flow angle θ is zero is now a singular point, so we shift the origin to H and multiply by -1 to obtain the χ plane, defined by

$$\chi = \frac{2N^2}{(N^4 - 1)u_0^2} - \lambda - \frac{N^4}{(N^4 - 1)^2 u_0^4 \lambda} = - \frac{(N^2 + 1)^2 (N^2 u_0^2 - \nu^2)^2}{(N^4 - 1)u_0^2(\nu^2 - u_0^2)(N^4 u_0^2 - \nu^2)} \qquad \ldots (3)$$

Taking the square root removes the singularity at H, making ABCHD straight in the plane of $\chi^{\frac{1}{2}}$. The remaining, hitherto undefined, portion DE of the boundary streamline may take various forms, dictated by analytical convenience.

One fairly simple assumption for DE is that in the $\chi^{\frac{1}{2}}$ plane it is a straight line perpendicular to AD. Suppose $(h, 0)$ are the coordinates of D in the $\chi^{\frac{1}{2}}$ plane. Then shifting the origin to D, and squaring, makes ABCDE a straight line in the plane of $\varepsilon = (\chi^{\frac{1}{2}} - h)^2$. Thus

$$w = J(\chi^{\frac{1}{2}} - h)^2 \qquad \ldots (4)$$

is the solution we require, and

$$z = \int \frac{dw}{\nu} = \int \frac{1}{\nu} \frac{dw}{d\chi} \frac{d\chi}{d\lambda} \frac{d\lambda}{d\nu} \, d\nu \qquad \ldots (5)$$

Now from equations (2) to (4)

$$\frac{d\lambda}{d\nu} = -\frac{2\nu}{(\nu^2 - u_0^2)^2},$$

$$\frac{d\chi}{d\lambda} = -1 + \frac{N^4}{(N^4 - 1)^2 u_0^4 \lambda^2} = -1 + \frac{N^4(\nu^2 - u_0^2)^2}{(N^4 u_0^2 - \nu^2)^2},$$

and $$\frac{dw}{d\chi} = J\left(1 - \frac{h}{\chi^{\frac{1}{2}}}\right)$$

$$= J\left[1 + \frac{ihu_0(N^4 - 1)^{\frac{1}{2}}(\nu^2 - u_0^2)^{\frac{1}{2}}(N^4 u_0^2 - \nu^2)^{\frac{1}{2}}}{(N^2 + 1)(N^2 u_0^2 - \nu^2)}\right],$$

so that (5) becomes

$$z = -2J\int\left[1 + \frac{iK(\nu^2 - u_0^2)^{\frac{1}{2}}(N^4 u_0^2 - \nu^2)^{\frac{1}{2}}}{N^2 u_0^2 - \nu^2}\right]\left[\frac{N^4}{(N^4 u_0^2 - \nu^2)^2} - \frac{1}{(\nu^2 - u_0^2)^2}\right]d\nu \qquad \text{... (6)}$$

where $$K = \frac{hu_0(N^4 - 1)^{\frac{1}{2}}}{N^2 + 1} \qquad \text{... (7)}$$

In the above discussion we have assumed that the point D at which the right angle occurs in the $\chi^{\frac{1}{2}}$ plane of Fig. 7 corresponds to a point on the circular-arc section of the hodograph. However if h or K is large enough, the right angle in the $\chi^{\frac{1}{2}}$ plane may correspond in the hodograph plane to a point between F and G in Fig. 8, where $\theta = -\frac{\pi}{2}$, or even to a point between G and E, where $\theta = 0$. In these latter cases, therefore, F rather than D represents the downstream end of the initial constant-pressure portion of the free streamline. As $K \to \infty$, D approaches E, and we obtain the Riabouchinsky case of Fig. 3. On the other hand if $K = 0$, D coincides with the point H at which $\theta = 0$, and the case reduces to the parallel-streamline model of Fig. 3. Since $\chi^{\frac{1}{2}} = h$ at the point D by definition,

$$K = i\left[\frac{N^2 u_0^2 - \nu^2}{(\nu^2 - u_0^2)^{\frac{1}{2}}(N^4 u_0^2 - \nu^2)^{\frac{1}{2}}}\right]_D,$$

where suffix D denotes conditions at D. If D is between H and F,

$\nu_D = Nu_0\left(\cos\theta_D - i\sin\theta_D\right)$, so that

$$K = -\frac{2N\sin\theta_D}{(N^4 + 1 - 2N^2\cos 2\theta_D)^{\frac{1}{2}}}$$

and K lies between 0 for $\theta_D = 0$ and $2N/(N^2 + 1)$ for $\theta_D = -\frac{\pi}{2}$. If D is between F and G, $\nu_D = nu_0 i$ so that

$$K = \frac{N^2 + n^2}{(n^2 + 1)^{\frac{1}{2}}(N^4 + n^2)^{\frac{1}{2}}}$$

and K lies between $2N/(N^2 + 1)$ for $n_D = N$ at F, and 1 for $n_D = 0$ at G. If D is between G and E, $\nu_D = nu_0$, so that

$$K = \frac{N^2 - n^2}{(1 - n^2)^{\frac{1}{2}}(N^4 - n^2)^{\frac{1}{2}}}$$

and K lies between 1 for $n_D = 0$ at G, and infinity for $n_D \to 1$ at E.

Along BC, $\theta = \frac{\pi}{2}$ and $q = nu_0$, where $0 \leqslant n \leqslant N$, q being zero at B and Nu_0 at C. Hence $\nu = -inu_0$ and from (6)

$$x = 0,\ y = -\frac{2J}{u_0^3}\int_0^n\left[1 + \frac{K(n^2+1)^{\frac{1}{2}}(N^4+n^2)^{\frac{1}{2}}}{N^2 + n^2}\right]\left[\frac{1}{(n^2+1)^2} - \frac{N^4}{(N^4+n^2)^2}\right]dn \qquad \ldots (8)$$

Similar relations are also valid along FG if the hodograph contains any portion of this line, i.e. if $K > 2N/(N^2+1)$. Then $\nu = inu_0$ along FG and

$$x = x_F,\ y = y_F + \frac{2J}{u_0^3}\int_n^N\left[1 + \frac{K(n^2+1)^{\frac{1}{2}}(N^4+n^2)^{\frac{1}{2}}}{N^2 + n^2}\right]\left[\frac{1}{(n^2+1)^2} - \frac{N^4}{(N^4+n^2)^2}\right]dn \ \ldots (9)$$

Equations (8) and (9) can easily be integrated numerically and if we put the plate height δ of Fig. 2 equal to unity, so that at C $y = y_c = \frac{1}{2}$, (8) defines J/u_0^3 in terms of N and K by an expression of the form

$$-\frac{J}{u_0^3} = \frac{1}{a(N) + Kb(N)} \qquad \ldots (10)$$

We assume the pressure of the rear face of the plate to be uniform, equal to that on CD or CF, so from Bernouilli's equation the drag coefficient

$$C_D = \frac{1}{y_c}\int_0^{y_c} (N^2 - n^2)\,dy$$

and may readily be evaluated. Similarly by putting $\nu = nu_0$, $0 \leqslant n \leqslant 1$, in (6) we may find x as a function of n, or in other words the pressure distribution, along the streamline AB approaching the plate and also along the part GD of the free streamline if $K > 1$ so that D lies between G and E. Along CD, or along CF if $K > 2N/(N^2+1)$, $\nu = Nu_0 e^{-i\theta}$. Hence

$$\frac{iK(\nu^2 - u_0^2)^{\frac{1}{2}}(N^4u_0^2 - \nu^2)^{\frac{1}{2}}}{N^2u_0^2 - \nu^2} = \frac{iK\left[(N^4 + 1)e^{-2i\theta} - N^2(1 + e^{-4i\theta})\right]^{\frac{1}{2}}}{N(1 - e^{-2i\theta})}$$

But $$1 + e^{-4i\theta} = 2e^{-2i\theta}\cos 2\theta$$

and $$1 - e^{-2i\theta} = 2i \sin\theta\, e^{-i\theta}$$

so that

$$\frac{iK(\nu^2 - u_0^2)^{\frac{1}{2}}(N^4u_0^2 - \nu^2)^{\frac{1}{2}}}{N^2u_0^2 - \nu^2} = \frac{K(N^4 + 1 - 2N^2\cos 2\theta)^{\frac{1}{2}}}{2N \sin\theta}$$

along CD or CF. Likewise

$$\frac{N^4}{(N^4u_0^2 - \nu^2)^2} - \frac{1}{(\nu^2 - u_0^2)^2} = \frac{1}{u_0^4}\left[\frac{1}{(N^2 - e^{-2i\theta})^2} - \frac{1}{(N^2e^{-2i\theta} - 1)^2}\right]$$

$$= -\frac{2i(N^4 - 1)\sin 2\theta e^{2i\theta}}{u_0^4(N^4 + 1 - 2N^2\cos 2\theta)^2}$$

since $e^{-4i\theta} - 1 = -2i \sin 2\theta e^{-2i\theta}$. Hence (6) becomes

$$x = -\frac{4J(N^4 - 1)N}{u_0^3}\int_\theta^{\frac{\pi}{2}}\left[1 + \frac{K(N^4 + 1 - 2N^2\cos 2\theta)^{\frac{1}{2}}}{2N \sin\theta}\right]\frac{\sin 2\theta \cos\theta\, d\theta}{(N^4 + 1 - 2N^2\cos 2\theta)^2}$$

and

$$y = y_c - \frac{4J(N^4 - 1)N}{u_0^3} \int_\theta^{\frac{\pi}{2}} \left[1 + \frac{K(N^4 + 1 - 2N^2\cos 2\theta)^{\frac{1}{2}}}{2N \sin \theta}\right] \frac{\sin 2\theta \sin \theta \, d\theta}{(N^4 + 1 - 2N^2\cos 2\theta)^2} \quad \ldots (11)$$

along CD or CF. These expressions can again be integrated numerically and from (10) it follows that they are of the form

$$x = \frac{A(N,\theta) + K\,C(N,\theta)}{a(N) + K\,b(N)}$$

$$y = \frac{1}{2} + \frac{B(N,\theta) + K\,D(N,\theta)}{a(N) + K\,b(N)}$$

Finally consider the portion DE of the boundary streamline. Here q and θ are both variable, and we have to use the relation $\psi = 0$ to define q or $n = q/u_0$ in terms of θ. From equations (3), (4), and (7), since ψ is the imaginary part of w, we require

$$\mathscr{I}\left[\frac{i(N^2u_0^2 - \nu^2)}{(\nu^2 - u_0^2)^{\frac{1}{2}}(N^4u_0^2 - \nu^2)^{\frac{1}{2}}} - K\right]^2 = 0$$

along ABCDE. Thus if

$$\frac{N^2u_0^2 - \nu^2}{(\nu^2 - u_0^2)^{\frac{1}{2}}(N^4u_0^2 - \nu^2)^{\frac{1}{2}}} = c + di \quad \ldots (12)$$

where c and d are real,

$$c(d + K) = 0.$$

Along ABCD, $c = 0$, and along DE

$$d = -K \quad \ldots (13)$$

If $(n^2\cos 2\theta - 1 + in^2\sin 2\theta)^{\frac{1}{2}}(N^4 - n^2\cos 2\theta - in^2\sin 2\theta)^{\frac{1}{2}} = e + fi$ it follows from (12) that

$$c = [e(N^2 - n^2\cos 2\theta) - f\, n^2\sin 2\theta]/(k\ell) \quad .. \quad (14)$$

and $$d = [f(N^2 - n^2\cos 2\theta) + e\, n^2\sin 2\theta]/(k\ell) \quad ... \quad (15)$$

where $$k = (n^4 + 1 - 2n^2\cos 2\theta)^{\frac{1}{2}}, \quad \ell = (N^8 + n^4 - 2N^4n^2\cos 2\theta)^{\frac{1}{2}} \quad ... \quad (16)$$

Also, since $(r \pm is)^{\frac{1}{2}} = \frac{1}{2^{\frac{1}{2}}}\left[(\sqrt{r^2 + s^2} + r)^{\frac{1}{2}} \pm i\,(\sqrt{r^2 + s^2} - r)^{\frac{1}{2}}\right]$,

$$e = \tfrac{1}{2}\Big[(k + n^2\cos 2\theta - 1)^{\frac{1}{2}}(\ell + N^4 - n^2\cos 2\theta)^{\frac{1}{2}} +$$
$$+ (k - n^2\cos 2\theta + 1)^{\frac{1}{2}}(\ell - N^4 + n^2\cos 2\theta)^{\frac{1}{2}}\Big] \quad ... \quad (17)$$

and $$f = \tfrac{1}{2}\Big[(k - n^2\cos 2\theta + 1)^{\frac{1}{2}}(\ell + N^4 - n^2\cos 2\theta)^{\frac{1}{2}} -$$
$$- (k + n^2\cos 2\theta - 1)^{\frac{1}{2}}(\ell - N^4 + n^2\cos 2\theta)^{\frac{1}{2}}\Big] \quad ... \quad (18)$$

A simple programme has been written for the ACE computer of Mathematics Division, NPL, to determine e, f, c, and d for any assumed values of n and θ. Thus for a given value of K, $\theta(n)$ can be found by cross-plotting the results for each value of n. The general form of the relationship is as shown in Fig. 9. For $K < 2N/(N^2+1)$ the path DE will be as (a), and along it n will in many cases decrease monotonically as θ increases from $-\theta_D$ to zero. For $2N/(N^2+1) < K < 1$, the path DE will be as (b), and n will initially decrease as θ increases above $-\theta_D$ (which is $-\frac{\pi}{2}$), and may become less than 1. Thus the pressure may rise above that in the free stream. Further increase of θ will cause n to increase again till it reaches a maximum, greater than 1. Then finally n will decrease again to 1 as θ tends to zero. For $K > 1$ the path DE will be still more complicated, as (c). Here n will initially be less than 1 and θ_D zero. As θ becomes negative along DE n will increase. The maximum negative angle will be reached at the point D', which is on the envelope of the intersections of the dotted lines for $0 < n < 1$. Along DD' the appropriate values for n will be those for the dotted curves of least slope. Then the path will return along D'E, the appropriate values for n now being initially those for the dotted curves of greatest slope, and subsequently those for the solid curves. Thus n increases to a maximum greater than 1 and finally decreases again to approach 1 as $\theta \to 0$. The corresponding streamline shapes in the physical plane are sketched on the right of the diagram.

For the downstream part of DE, where θ increases towards zero and n decreases to 1, θ will become small, much less than n^2-1, and it follows then from (13) to (18) that

$$\theta \to -\frac{K(n^2-1)^{3/2}(N^4-n^2)^{3/2}}{n^2(n^2+N^2)(N^2-1)^{\frac{1}{2}}} \quad \ldots (19)$$

The computer results however give θ all along DE and also give the corresponding values of c. Now $z = \int dw/v$ and from (3), (4), (7), (12) and (13), $w = -J(N^2+1)/c^2/[(N^2-1)u_0^3]$. Hence along DE

$$x = x_D - \frac{J(N^2+1)}{(N^2-1)u_0^3}\int_0^{c^2} \frac{\cos\theta}{n} d(c^2)$$

and $$y = y_D - \frac{J(N^2+1)}{(N^2-1)u_0^3}\int_0^{c^2} \frac{\sin\theta}{n} d(c^2),$$

c being zero at D. These equations can be integrated numerically once θ and n have been found as functions of c^2. Far downstream where $n \to 1$ and $\theta << n^2-1$ it follows from (14) to (19) that

$$c^2 \to \frac{N^2-1}{(N^2+1)(n^2-1)} \text{ and } \frac{\sin\theta}{n} \to -K\left(\frac{N^2+1}{N^2-1}\right)^{\frac{1}{2}}(n^2-1)^{3/2}$$

Hence

$$(y)_{n=1+\varepsilon} - y_E = -\frac{2JK}{u_0^3}\left\{\frac{2(N^2+1)}{N^2-1}\right\}^{\frac{1}{2}} \varepsilon^{\frac{1}{2}} \quad \ldots (20)$$

where ε is small and y_E is half the ultimate wake thickness. From equation (1), since we have put $\delta = 1$, the ultimate wake thickness should be $\frac{1}{2}C_D$. In general this will not be equal to $2y_E$ as calculated from the above analysis, but for any given value of N there will be equality for one value of K, which may therefore be taken to be the correct one.

The above solution may be termed the converging-streamline model to distinguish it from the models of Fig. 3, though as pointed out above both the parallel-streamline model and the Riabouchinsky model may be obtained from it as special cases by putting $K = 0$ and ∞ respectively and abandoning condition (1) for the downstream wake thickness. It is however not the only possible model with a partially necking-in wake. We assumed above that in the $\chi^{\frac{1}{2}}$ plane in Fig. 7 the line DE is straight and perpendicular to AD. Another analytically manageable possibility would be to assume that the streamline pattern in the $\chi^{\frac{1}{2}}$ plane is that corresponding to a uniform stream parallel to AD combined with, on AD produced, a source whose strength and position are such as to make D a stagnation point, as in Fig. 10. Such a flow would then be characterised by three parameters, (i) the velocity ratio N on CD, (ii) the maximum negative flow angle defining the position of D, and (iii) the source strength. The equation corresponding to (4) for the complex velocity potential would be

$$w = L\left\{\left(\chi^{\frac{1}{2}} - h\right) + M \log\left[1 - \frac{\chi^{\frac{1}{2}} - h}{M}\right]\right\} \qquad \ldots (21)$$

For an infinitely strong source, which would have to be situated at an infinite distance to the right on Fig. 10 to make D a stagnation point, the line DE in the $\chi^{\frac{1}{2}}$ plane would be straight, perpendicular to AD, and the case would reduce to the converging-streamline model. For a source of zero strength situated at D, the line ADE would already be straight in the $\chi^{\frac{1}{2}}$ plane, and the case would reduce to the Riabouchinsky model. The forms taken by DE in the hodograph plane would resemble those sketched in Fig. 11, where a, b, c, and d show respectively the converging-streamline model, a strong source case, a moderate source case, and the Riabouchinsky model. As with the converging-streamline model it would not be very difficult to determine the shape of the constant-pressure portion CD of the free streamline for this source model. However the determination of the downstream shape DE would be difficult, since the condition $\psi = 0$ obtained from (21) would be very complicated. Unless, therefore, comparison with experiment shows that a three-parameter method is essential to give an adequate representation of real flows, it would not seem to be worthwhile pursuing this source model further.

The converging-streamline model satisfying the downstream wake-thickness condition has been evaluated for two cases, $N = 1.5$ and 1.2.

Results are shown in Figs 12 and 13 in comparison with those for the Riabouchinsky and parallel-streamline models. For $N = 1.5$, $C_D = 2.00$, irrespective of K, so that the downstream wake-thickness condition is $y_E = 0.50$. This was found to be satisfied with D between H and F in Fig. 8. the flow being of the form (a) of Fig. 9 with $K = 0.596$ and $\theta_D = -18°$. For $N = 1.2$, $C_D = 1.27$, again irrespective of K, so that $y_E = 0.32$, a condition requiring D to be between F and G in Fig. 8, the flow being of the form (b) of Fig. 9, with $K = 0.998$. For $N = 1.5$ the angle θ_D represents the maximum convergence towards the centre line, and persists only over a very short region. Well downstream of D the streamlines converge only very slowly towards the axis, as is implied by equation (20). It is worth noting that the results in Figs 12 and 13 for the parallel-streamline model show a considerably shorter region of constant pressure than the calculations of Roshko[6], though they agree with the results of Gerber and McNown[7]. Apparently Roshko made an error in his analysis. The comparison of the converging-streamline results of Figs 12 and 13 with experiment is discussed below.

4. EXPERIMENTAL RESULTS FOR FLOW IN AIR

There are few experimental results for flow past a normal flat plate either in cavitating or non-cavitating flow. In the air-flow experiments of Fage and Johansen[14] detailed measurements were made close to the plate, but they did not extend far downstream. Likewise Fail, Lawford, and Eyre[12] were primarily concerned with finite aspect-ratio plates, and made no detailed measurements for the two-dimensional case. Accordingly it was decided to make some new measurements in the 7 ft wind tunnel of Aerodynamics Division, NPL. This tunnel has a working section approximately 7 ft square in cross section, with fillets in the corners. A steel bar, 7 ft long, 2.5 inches in width, and 0.73 in thick was mounted centrally in the tunnel broadside to the flow with its length horizontal. The air-speed was 80 ft/sec giving a Reynolds number based on the 2.5 in dimension of about 1.1×10^5. At such Reynolds numbers the flow in the wake is turbulent, and the drag coefficient is about 2. We hoped to find, therefore, some correspondence with the models of Fig. 12, where C_D is also 2.

The main series of experiments consisted of traversing a static-pressure tube behind the bar or plate by means of a traverse mechanism mounted on the tunnel floor. The static tube used was of the spade-shaped type due to Girerd and Guienne[15], as shown in Fig. 14. It was made from hypodermic tube flattened and honed at the end. Its advantages are that the measured holes are near the tip and also that the pressure it records is insensitive to cross flows in the plane of the tip edge and the tube axis. For the present experiments it was used with its axis parallel to the undisturbed stream and its tip edge vertical. This permitted the static-pressure field behind the plate to be mapped without first making detailed flow-direction measurements, as would have been necessary with a conventional static tube which needs to be aligned with the local flow. Despite the divergence of the streamlines from the axis in the close vicinity of the plate and their convergence further downstream, the fixed-direction static tube used should give only small errors. Moreover it should perhaps give a more correct mean value of the pressure in the fluctuating flow than a conventional tube, since the fluctuations in the flow direction are primarily in a vertical plane and should have relatively little effect on the readings. By contrast, a conventional tube is affected by direction fluctuations as well as by pressure fluctuations.

Results of the measurements are shown in Fig. 15 in the form of plottings of the lines of constant pressure. The unit of length is the 2.5 in dimension of the plate. In the corresponding theoretical case of Fig. 12, C_p is initially equal to -1.25 along the free streamlines through the plate edges, and it can be seen that the predicted free-streamline shapes near to the plate are indeed broadly similar to the -1.25 isobar in Fig. 15. If however one were to plot the free streamlines of Fig. 12 on to Fig. 15, and thus determine the pressure distributions in the real flow along lines whose coordinates are the same as those of the theoretical free streamlines, the resulting pressure distributions would not resemble very closely the theoretical distributions of Fig. 12, though the discrepancy would be smallest for the converging-streamline model. In the real flow low pressures persist a long way downstream near the axis. This is due to the vortex-street effect discussed in Section 2, where it was pointed out that agreement between theory and experiment can only be expected outside the region of frictional effects. The limits of this region were found experimentally by traversing a pitot tube across the wake. Far from the axis the pitot pressure is the same as in the undisturbed stream but within the wake there is a loss of pitot pressure. The dotted boundary in Fig. 15 is where appreciable pitot losses were first detected when traversing the probe towards the axis. Ideally, therefore, only the pressure field outside this boundary should be compared with the predictions of the theories. However it would be very laborious to evaluate the theoretical pressure field in these outer regions.

A few spot measurements were made with a yawmeter to determine mean flow angles. The maximum recorded angle of convergence towards the axis was at $x = 1.6$, $y = 0.70$, and was 19°. This, as it happens, is close to the maximum convergence angle of 18° in the converging-streamline model of Fig. 12, though again, at such a position within the region of frictional effects, agreement between theory and experiment is not necessarily to be expected.

Thus we can only say that the converging-streamline model is probably a rather better representation of the real flow than the other two models. It seems pointless investigating any more complicated models in the hope of getting still better agreement since it is impossible to make any very precise comparisons with experiment unless one is prepared to go to the great labour of computing the pressure distribution over the outer regions of the flow field.

If we provisionally accept the conclusion that the converging-streamline model is an adequate representation of real non-cavitating turbulent-wake flow past a plate, we still cannot claim to have provided a complete theoretical solution of the problem, since we do not know theoretically what the base pressure ought to be. Thus N, the velocity ratio on the upstream part of the free streamline in Fig. 12, is a parameter assumed in the calculations. For smaller assumed values of N, the constant-pressure region of the free streamlines is predicted to be longer, as can be seen from Fig. 13. Physically this length at constant pressure must correspond to the length required before occasional violent incursions of lumps of fluid to the central regions of the wake can take place. If, therefore, one could consider theoretically the amplification of the instabilities in the separated shear layers, it might be possible, using the converging-streamline model, to predict the drag coefficient. However such an instability theory is beyond the powers of the author.

It is simpler to consider a case with a long splitter plate along the centre line of the wake behind the plate, as in Fig. 16. Here the large-scale eddying motions should be mostly suppressed. The flow in the shear layers springing from the plate will be turbulent at sufficiently high Reynolds numbers and then, if there are no large-scale eddies, the shear-layer thickness s should increase approximately linearly with distance downstream as shown. Suppose that the velocity just outside the shear layer is u_1, and that it is u_2 between the layer and the splitter plate. The latter velocity will be negative since there will be reversed flow, but probably $|u_2|$ will be much less than u_1. If the boundaries of the shear layer are taken as the points where $(u-u_2)/(u_1-u_2)$ is equal to 0.05 and

0.95, the thickness s of the layer should be approximately equal to 0.18x according to results of Reichardt presented in Fig. 23.3 of Ref. 17. We may plausibly assume that the centre line CD of the shear layer should coincide with the constant-pressure part of the free streamline as calculated according to the converging-streamline model for the experimentally observed base pressure. Further it is reasonable to suppose that in the real flow the pressure will remain constant until the inner boundary of the shear layer strikes the plate, since upstream of this point the air between the shear layer and the splitter plate will be fairly slow-moving. Hence we should have $y_D = 0.09x_D$ for the corresponding converging-streamline model. This will only be true for one velocity ratio N. Thus for the case N = 1.5 of Fig. 12, where $C_D = 2.00$, $y_D = 0.71x_D$, whilst for the case N = 1.2 of Fig. 13, where $C_D = 1.27$, $y_D = 0.14x_D$. It appears, then, that N should be a little less than 1.2, so that the theoretically predicted drag coefficient for a normal flat plate with a long splitter plate would be about 1.2. The experimental result of Ref. 18 is $C_D = 1.38$. The discrepancy between this and the predicted value is probably not excessive in view of the crude way in which the turbulent shear-layer analysis has been combined with the inviscid converging-streamline model. In particular the analysis seems dubious where, as in Fig. 13, the free streamline is predicted to have a portion normal to the axis. However the experimental measurements show that the maximum rate of decrease of displacement thickness occurs at about 8 plate heights downstream of the plate, and it is precisely here that the vertical part of the free streamline occurs in Fig. 13. Thus the experimental flow pattern is in reasonable harmony with a converging-streamline model whose drag coefficient is not far from the correct value.

5. CAVITATING FLOWS

Strange though it may seem, hardly any experiments have been done on cavitating liquid flow past a normal two-dimensional plate. The only results known to the author are those presented in the excellent paper of Reichardt[19], and in the more recent paper of Waid[20]. Reichardt shows measurements of the ratio of the maximum cavity width to the plate height, plotted as a function of cavitation number σ, which is equal to minus the pressure coefficient in the cavity. In our notation $\sigma = N^2-1$. If N is very close to 1, equal to $1 + \alpha$, $\sigma = 2\alpha$. Equation (8) then shows that for a plate height of unity $(y_c = \frac{1}{2})$

$$\int_0^1 \frac{(1-n^2)dn}{(1+n^2)^{\frac{3}{}}} = -\frac{u_0^3}{16J\alpha} \quad \text{for} \quad K = 0$$

$$= -\frac{u_0^3}{16JK\alpha} \quad \text{for} \quad K \to \infty$$

The left-hand side here is $(4+\pi)/16$. Further, since $N^4+1-2N^2\cos 2\theta \approx 4(\sin^2\theta+\alpha^2)$, where the term in α^2 is retained since $\sin\theta$ may be zero, equation (11) shows that at the point of maximum cavity thickness, where $\theta = 0$,

$$y = y_c - \frac{16J\alpha}{u_0^3} \int_{\theta=0}^{\frac{\pi}{2}} \frac{2\sin^2\theta\alpha(\sin\theta)}{16(\sin^2\theta + \alpha^2)^{\frac{}{2}}} \quad \text{for} \quad K = 0$$

$$\to \frac{\pi}{2(4+\pi)\alpha} \quad \text{as} \quad \alpha \to 0.$$

Hence the ratio of the plate height to the maximum cavity thickness $2y$ is

$$r = r_0 = \frac{(4+\pi)\sigma}{2\pi} \qquad \dots (22)$$

for the parallel-streamline case $K = 0$. Similarly for the Riabouchinsky case $K \to \infty$, it follows from (11) that at the point of maximum cavity thickness

$$y = y_c - \frac{16JK\alpha}{u_0^3} \int_{\theta=0}^{\frac{\pi}{2}} \frac{d(\sin^2\theta)}{16(\sin^2\theta + \alpha^2)^{3/2}}$$

so that $y \to \frac{2}{(4+\pi)\alpha}$ as $\alpha \to 0$.

Hence here the ratio of the plate height to the maximum cavity thickness is

$$r = r_0 = \frac{(4+\pi)\sigma}{8} \qquad \dots (23)$$

Fig. 12 of Reichardt's paper shows that for σ in the range 0.035 to 0.10, the graph of r as a function of σ is approximately a straight line of slope slightly less then 1. From equations (22) and (23) it would therefore seem that the Riabouchinsky model represents the maximum cavity thickness more accurately than the parallel-streamline model. For low values of σ, the maximum cavity thickness according to the converging-streamline model will be practically the same as in the Riabouchinsky model. Hence Reichardt's experiments are at least not inconsistent with the converging-streamline model. However Waid's experiments appear at first sight to contradict it.

Reichardt's results were obtained in a free-jet tunnel in which the upper and lower boundaries were free, and the lateral boundaries were formed by parallel walls. The jet cross section was 15 × 20 cms, and the heights of the plates used were 0.5 and 1.5 mm. Thus $^{\delta}/h$, where h is the tunnel height, did not exceed 0.01. Waid's experiments were done in a solid-wall tunnel of cross section 14 × 2.9 ins, with a plate height of 0.375 in, so that $^{\delta}/h = 0.027$. For a given cavitation number Waid's configuration would have been subject to much greater blockage effects than Reichardt's, both because of the greater relative model size and because a solid-wall tunnel is worse in its effects on cavity size than an open-jet one, as can be seen from Fig. 4 of Ref. 21. Waid found that at high cavitation numbers, in the region of 1, the cavity width agreed with the predictions of the Riabouchinsky model for unrestricted flow, but at lower cavitation numbers, in the region of 0.5, the cavity was wider than predicted by the Riabouchinsky model. On the face of it, the results at high cavitation numbers seem to show that the Riabouchinsky model is to be preferred to the converging-streamline model, which at such cavitation numbers predicts a rather thinner cavity. However it is not clear how much Waid's results, even at the high cavitation numbers, were affected by tunnel blockage, which was certainly very important for $\sigma = 0.5$. It would therefore be useful to do further experiments with very small models, perhaps in a slotted-wall tunnel. These should extend to high cavitation numbers to discriminate between the Riabouchinsky and converging-streamline models. We hope to be able to do such experiments in the fairly near future.

6. CONCLUDING REMARKS

One of the purposes of the present paper has been to stress the limitations inherent in free-streamline models as representations of real flows. A fully accurate representation is too much to hope for, but it would seem that the way towards an improvement lies in taking more adequate account of the physical processes operating in the wake. The converging-streamline model proposed only does this in the most elementary way, insofar as it represents correctly the displacement thickness far downstream. Nevertheless it seems to give a rather better representation of non-cavitating flow than is given by the parallel-streamline model or the Riabouchinsky model. For cavitating flows there is some limited evidence that at very low cavitation numbers both the Riabouchinsky model and the converging-streamline model are satisfactory. To discriminate between the two models experiments at higher cavitation numbers are needed. It may then possibly turn out that neither model represents the real flow very closely over the whole range of cavitation numbers. The physical arguments presented in Section 2 above, that the wake should be treated as having a downstream thickness related to the drag, will, however, remain valid, and to obtain an improved model it will be necessary to try and satisfy some of the other conditions imposed by the physical processes occurring in the wake. This will require more complicated models with converging wake streamlines. However the effort required to develop such models does not seem to be worthwhile until and unless experiment proves it to be desirable.

7. LIST OF SYMBOLS

c	defined by equation (12)
C_D	drag coefficient $D/(\frac{1}{2}\rho u_0^2\delta)$
C_p	pressure coefficient $(p-p_o)/(\frac{1}{2}\rho u_0^2)$
d	defined by equation (12)
D	drag per unit span
e	defined by equations (16) and (17)
f	defined by equations (16) and (18)
J	constant of dimensions length $\times$ (velocity)^3 defining scale of free-streamline model
K	constant related to amount of necking-in of free streamlines for convergent-streamline model
n	q/u_o
N	n on upstream part of free streamline
p	pressure
p_o	undisturbed free-stream pressure
q	fluid speed
r	ratio of plate height to maximum cavity thickness
t	separation of free streamlines as in Fig. 2

u	x-component velocity
u_o	undisturbed free-stream velocity
v	y-component velocity
w	complex potential $\phi + i\psi$
x	axial distance downstream of centre of plate
y	transverse distance from x-axis
z	$x + iy$
α	$N - 1$
δ	plate height as in Fig. 2: taken to be unity in much of the analysis
δ^*_w	wake-displacement thickness
θ	flow inclination to x axis
κ	strength of vortices in vortex street
λ	complex quantity defined by equation (2)
ν	$u - iv$
ρ	density
σ	cavitation number, $N^2 - 1$
ϕ	velocity potential
χ	complex quantity defined by equation (3)
ψ	stream function

REFERENCES

1. PARKIN, B. R. - Experiments on circular arc and flat plate hydrofoils. J. Ship Res., Vol. 1, No. 4, p.34, March 1958.
2. ROSHKO, A. - On the drag and shedding frequency of two-dimensional bluff bodies. N.A.C.A. TN 3169, July 1954.
3. NASH, J. F. - A review of research on two-dimensional base flow. A.R.C. R.& M. 3323, March 1962.
4. RIABOUCHINSKY, D. - On steady fluid motion with free surfaces. Proc. Lond. Math. Soc., Vol. 19, p.206, 1920.
5. BIRKHOFF, G. and ZARANTONELLO, E. H. - Jets, wakes, and cavities. Academic Press, New York, 1957.
6. ROSHKO, A. - A new hodograph for free streamline theory. N.A.C.A. TN 3168, July 1954.
7. GERBER, R. and McNOWN, J. S. - Transition curves of constant pressure. I. Streamlined struts. State University of Iowa, Studies in Engineering Bulletin, Vol. 35, p. 15, 1953.
8. BIRKHOFF, G. - Jets, wakes, and cavities. p.261 of Proceedings of Second Symposium on Naval Hydrodynamics, Office of Naval Research, Department of the Navy, ACR-38, 1958.
9. THWAITES, B. (editor) - Incompressible aerodynamics. Clarendon Press, Oxford, 1960.
10. WOODS, L. C. - Two dimensional flow of a compressible fluid past given curved obstacles with infinite wakes. Proc. Roy. Soc. A., Vol. 227, p. 367, 1955.
11. GOLDSTEIN, S. (editor) - Modern developments in fluid dynamics. Clarendon Press, Oxford, 1938.
12. FAIL, R., LAWFORD, J. A., and EYRE, R. C. W. - Low-speed experiments on the wake characteristics of flat plates normal to an air stream. A.R.C. R.& M. 3120, June 1957.
13. RUTHERFORD, D. E. - Fluid dynamics. Oliver and Boyd, 1959.
14. FAGE, A. and JOHANSEN, F. C. - On the flow of air behind an inclined flat plate of infinite span. R.& M. No. 1104, 1927.
15. GIRERD, H. and GUIENNE, P. - Nouvelles sondes de pression statique pour mesures aerodynamiques. C.R. Acad Sci., Paris, Vol. 228, p. 651, 1949.

16. HOERNER, S. F. - Fluid-dynamic drag. Published by the Author, 1958.

17. SCHLICHTING, H. - Boundary layer theory. Pergamon Press, London, 1955.

18. ARIE, M. and ROUSE, H. - Experiments on two-dimensional flow over a normal wall. J. Fluid Mech., Vol. 1, p. 129, 1956.

19. REICHARDT, H. - The physical laws governing the cavitation bubbles produced behind solids of revolution in a fluid flow. Paper of the Kaiser Wilhelm Institute for Hydrodynamical Research, Göttingen, October 1945: TPA3/TIB Translation Acsil/49/1499.

20. WAID, R. L. - Water tunnel investigation of two-dimensional cavities. Hydrodynamics Laboratory Report No. E-73.6, Cal. Inst. of Tech., September 1957.

21. COHEN, H. and DI PRIMA, R. C. - Wall effects in cavitating flows. p. 367 of Proceedings of Second Symposium on Naval Hydrodynamics, Office of Naval Research, Department of the Navy, ACR-38, 1958.

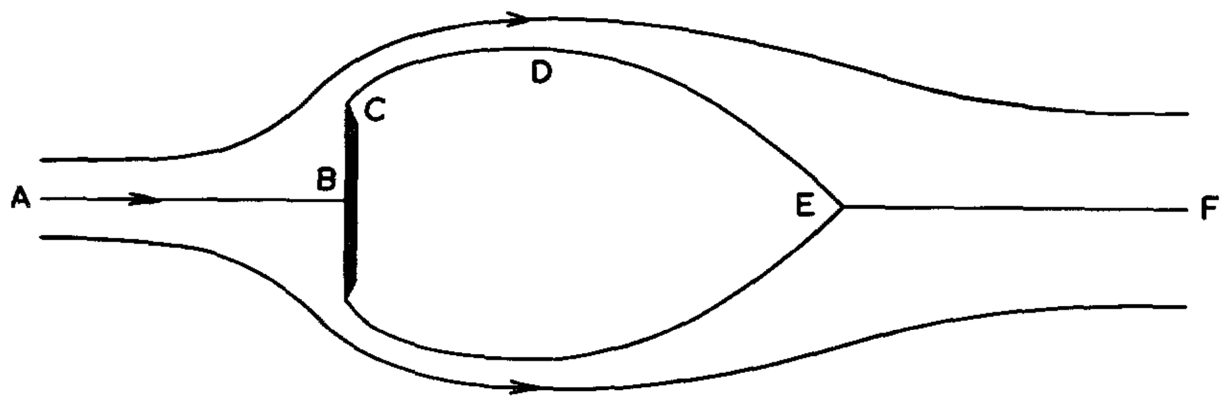

FIG 1 MEAN-FLOW STREAMLINES IN FLOW PAST A PLATE

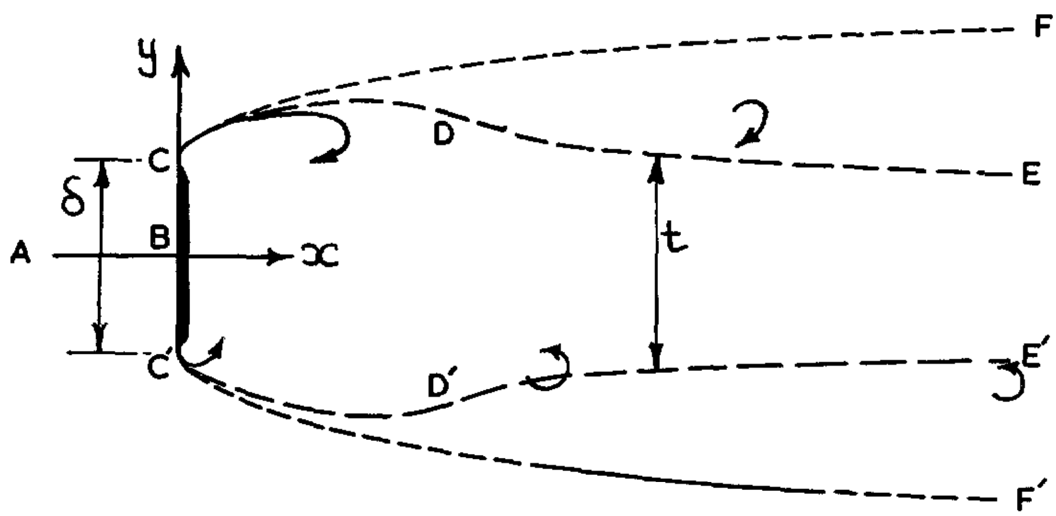

FIG 2 THE WAKE FLOW

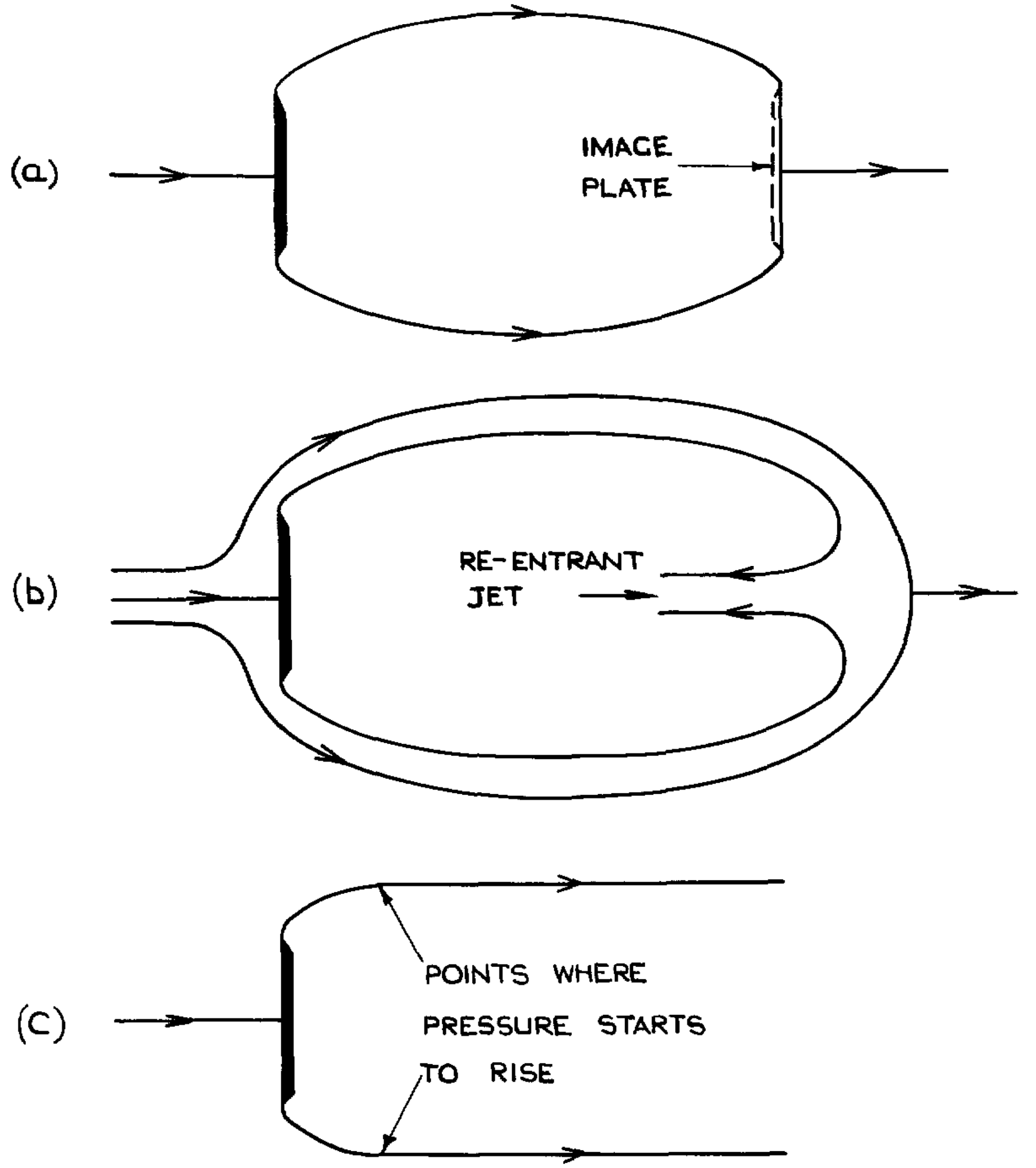

FIG 3 EARLIER FREE-STREAMLINE MODELS:
(a) RIABOUCHINSKY (b) RE-ENTRANT JET
(c) PARALLEL STREAMLINE

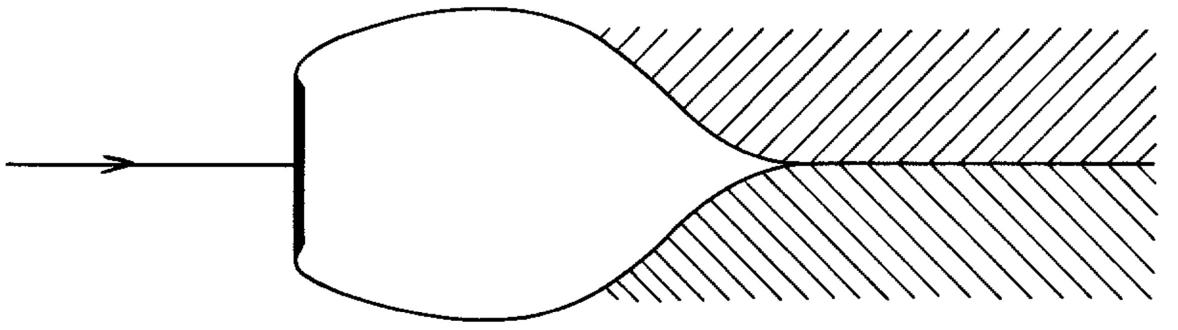

FIG 4 CUSPED CAVITY

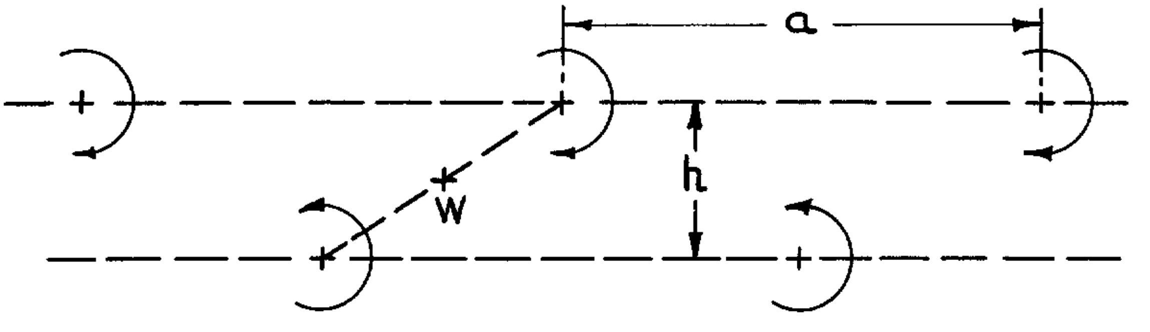

FIG 5 VORTEX STREET

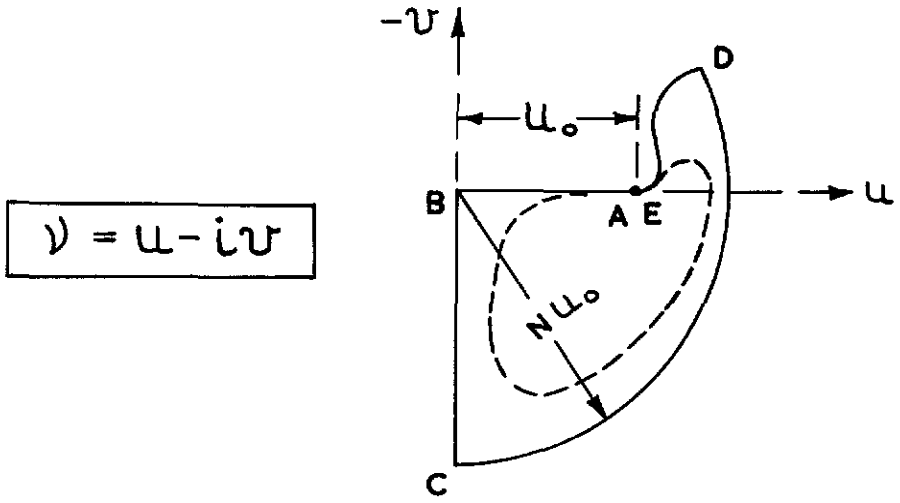

FIG 6 HODOGRAPH OF POSSIBLE MODEL

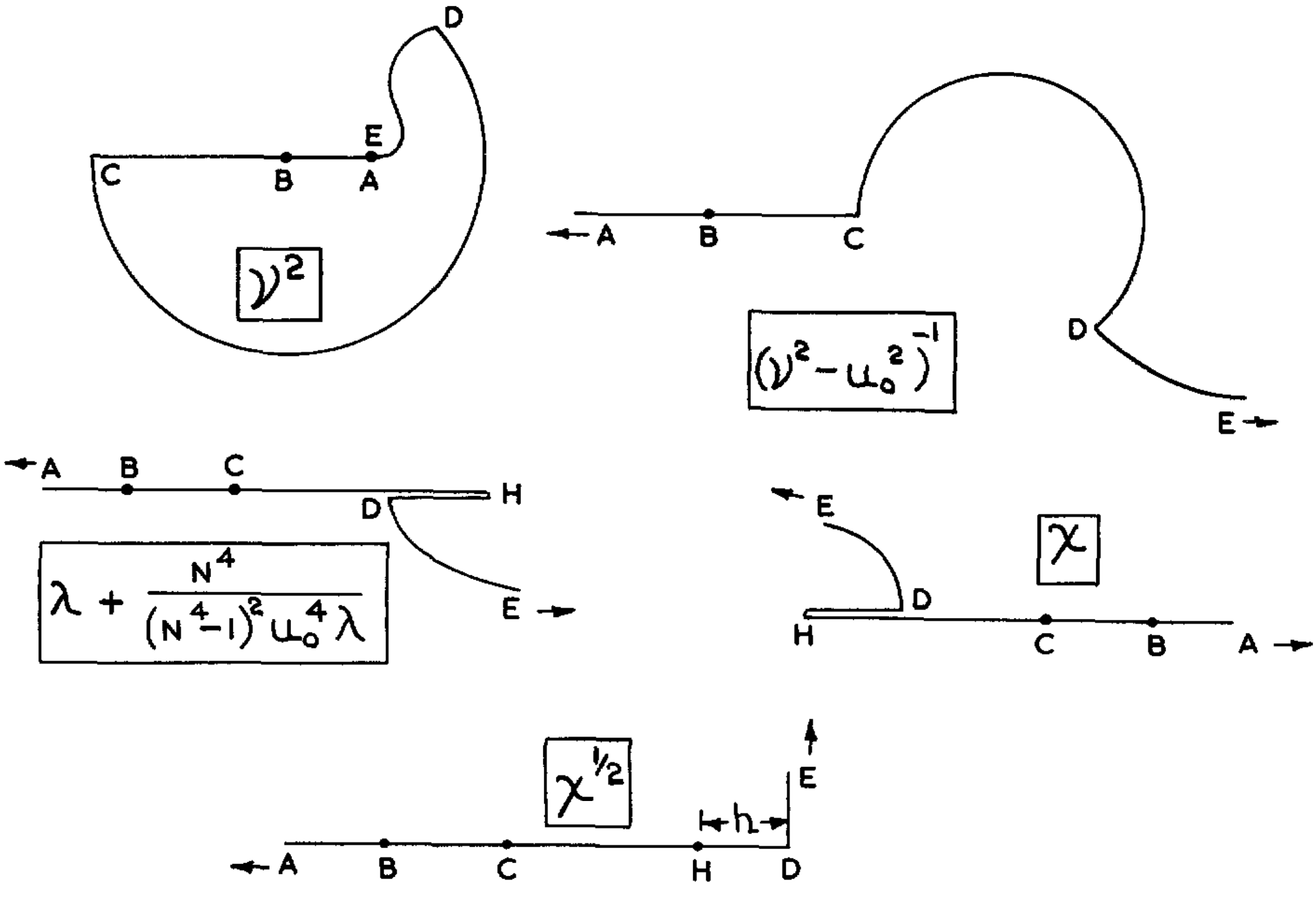

FIG 7 TRANSFORMATIONS OF HODOGRAPH PLANE

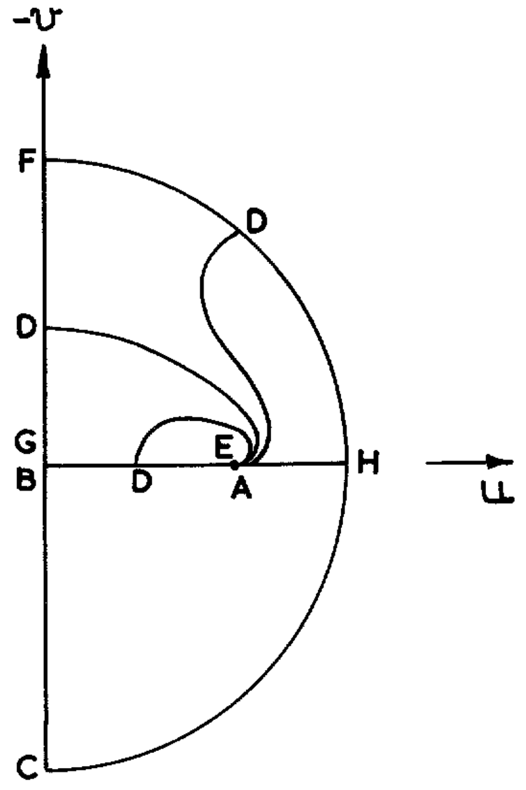

FIG.8 POSSIBLE POSITIONS OF D

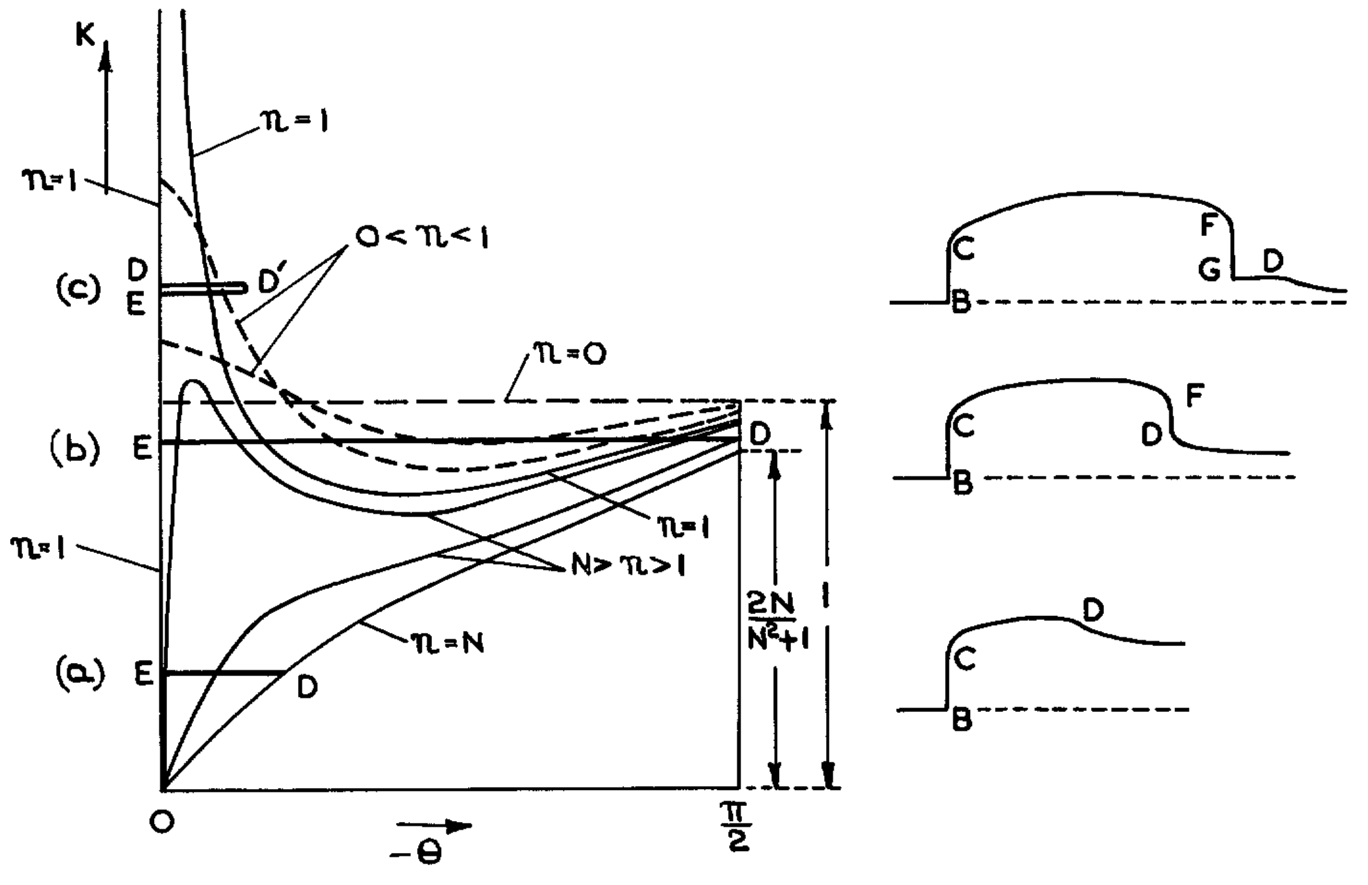

FIG.9 RELATION BETWEEN n, θ AND K

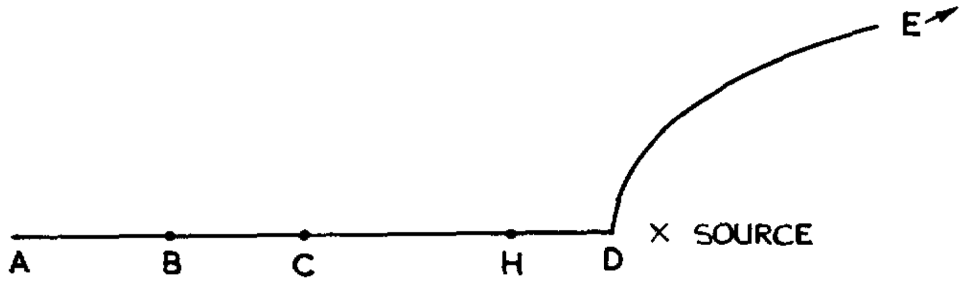

FIG 10 SOURCE IN $\chi^{1/2}$ PLANE

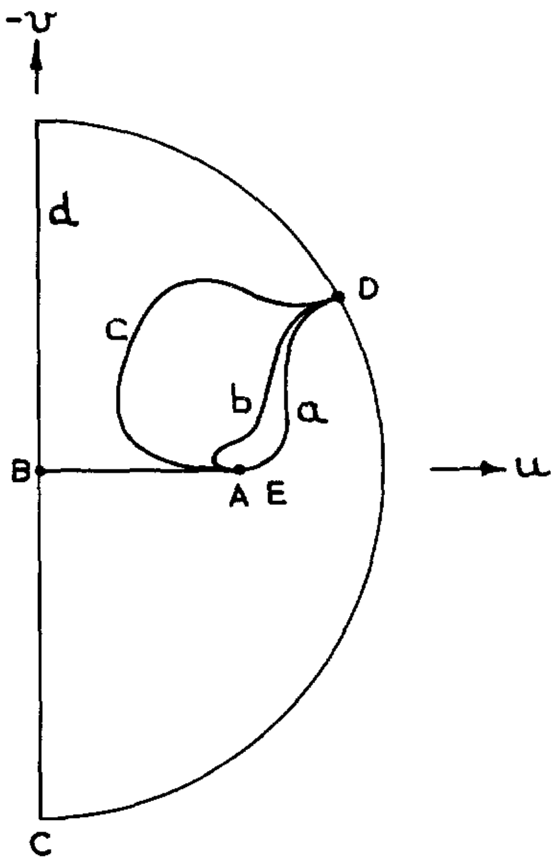

FIG.11 HODOGRAPH PLANE FOR VARIOUS SOURCE STRENGTHS

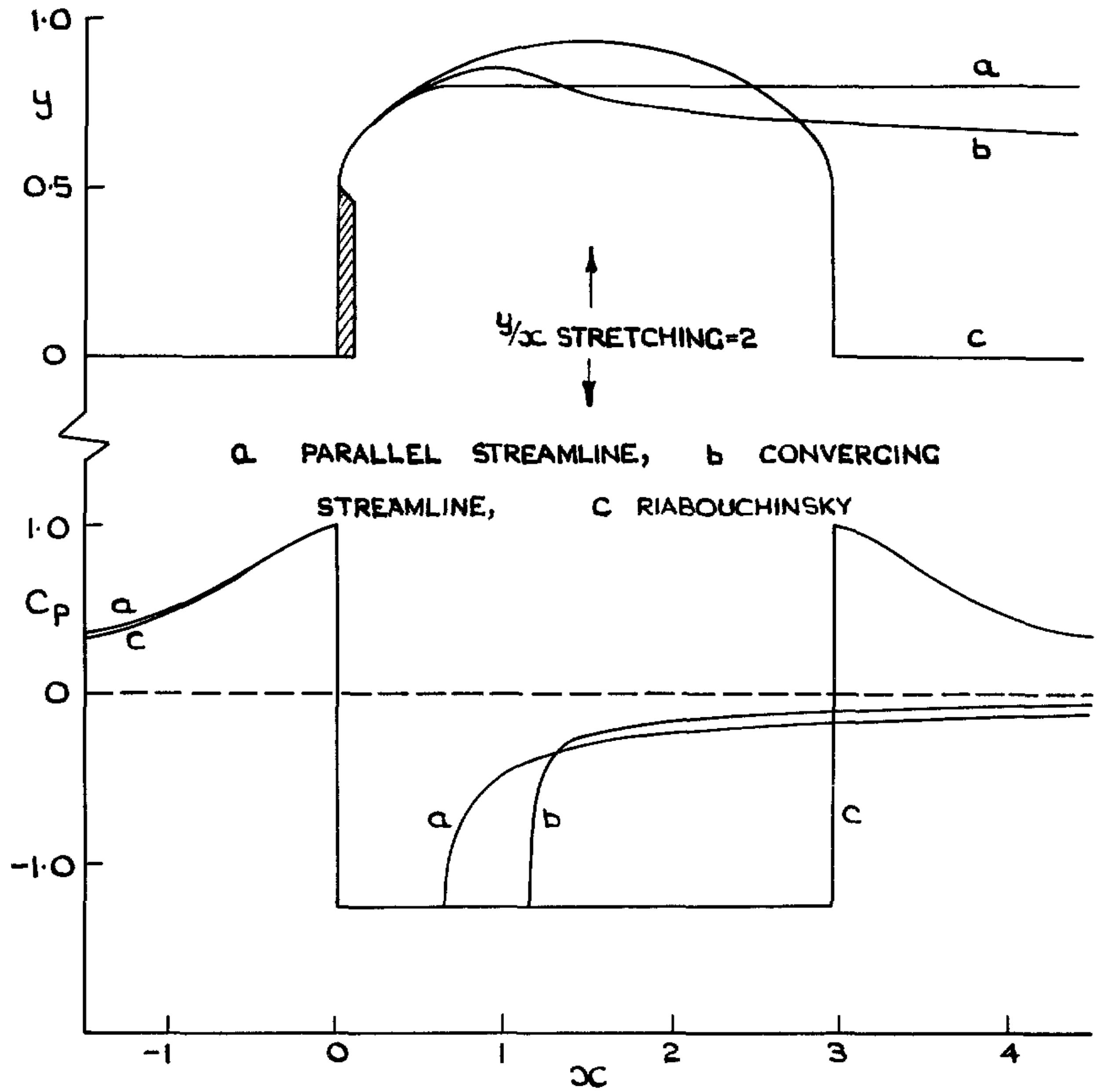

FIG. 12 SHAPES OF, AND PRESSURE DISTRIBUTIONS ALONG, FREE STREAMLINES FOR N = 1·5

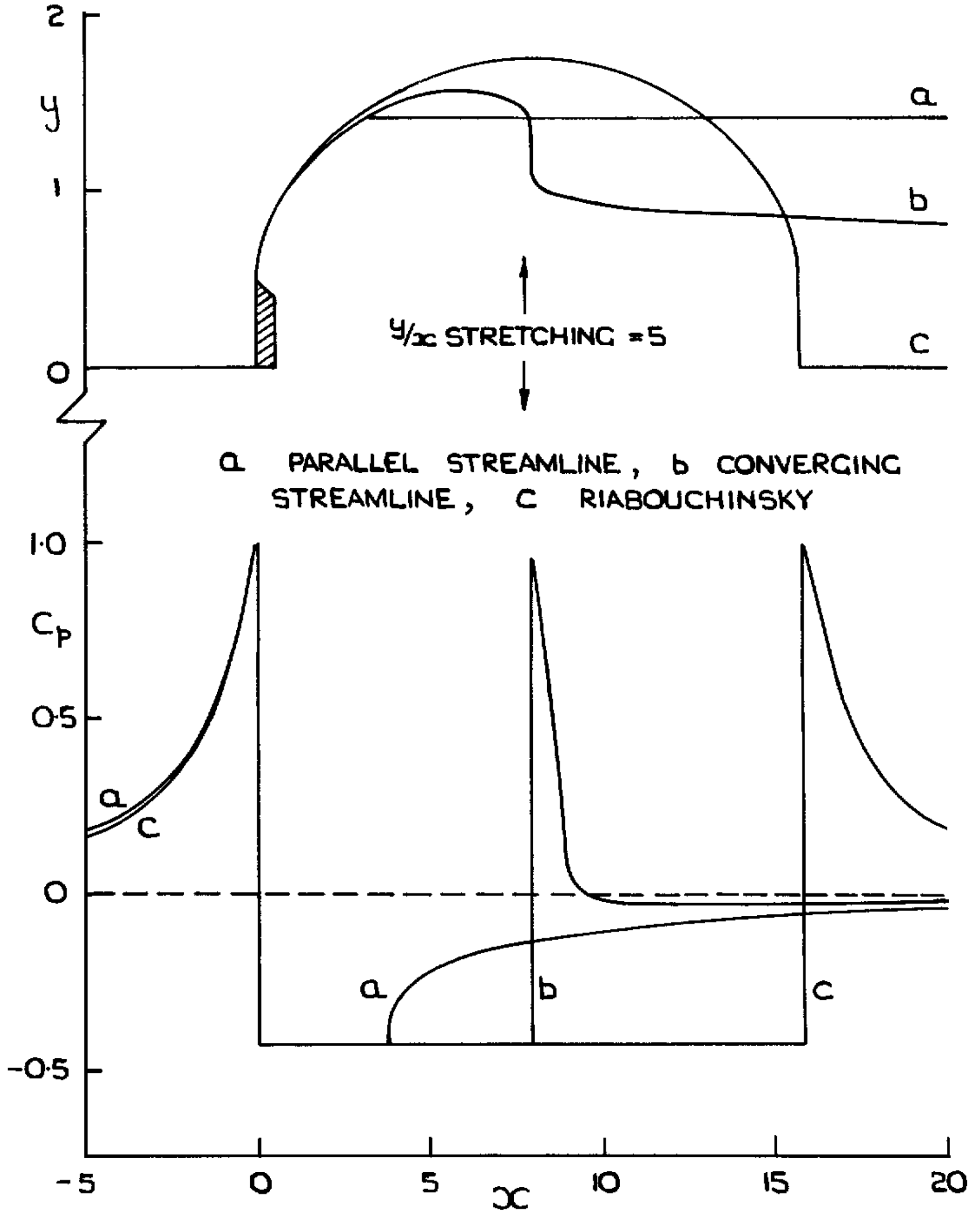

FIG. 13 SHAPES OF, AND PRESSURE DISTRIBUTIONS ALONG, FREE STREAMLINES FOR N = 1·2

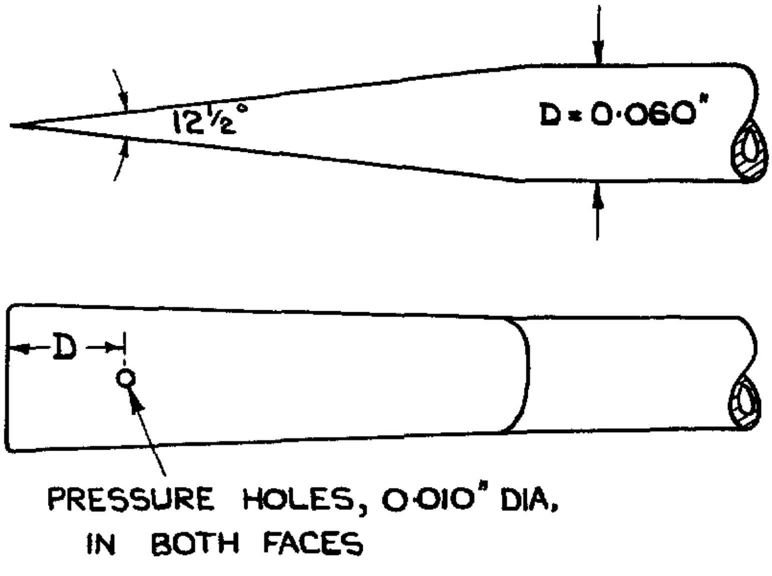

FIG. 14 STATIC TUBE USED

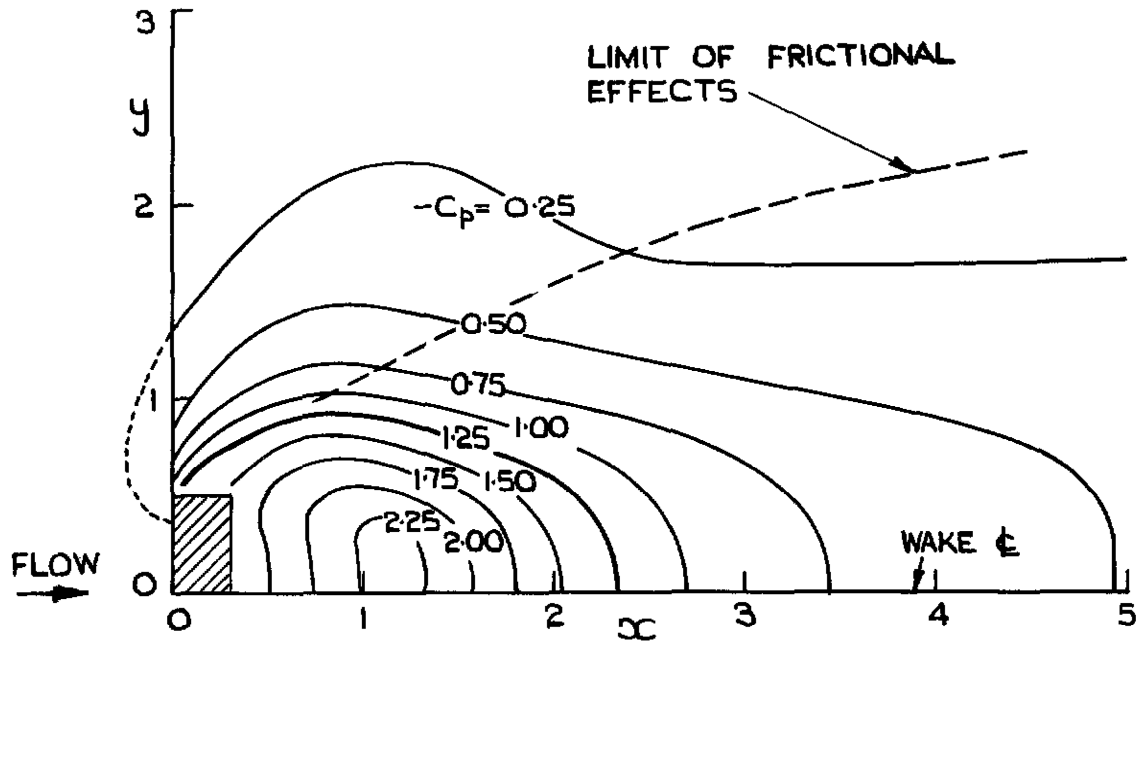

FIG. 15 ISOBARS IN AIR FLOW PAST A PLATE

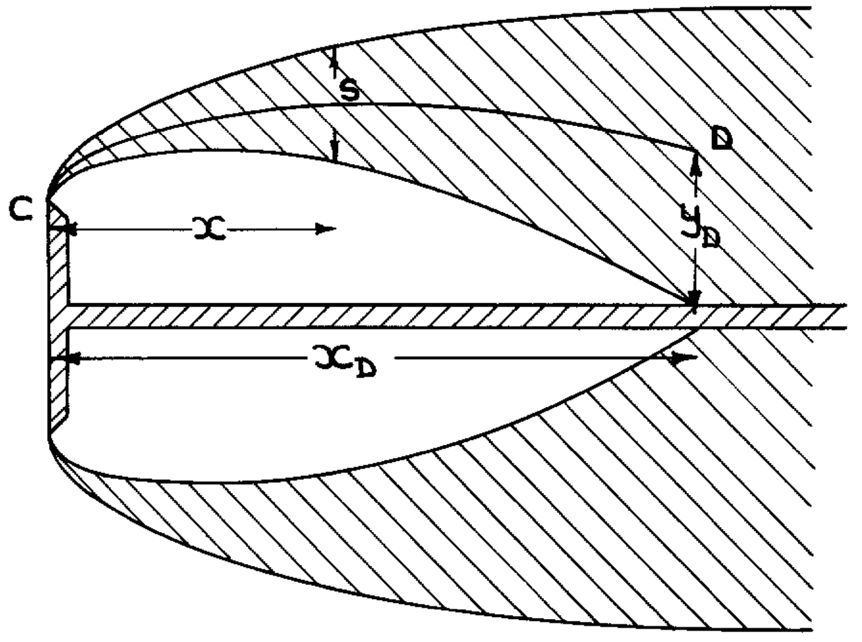

FIG 16 FLOW WITH LONG SPLITTER PLATE

A.R.C. C.P. No.697
November, 1962
Gadd, G. E. Ship Division, Nat. Phys. Lab.

TWO-DIMENSIONAL SEPARATED OR CAVITATING FLOW PAST A FLAT PLATE NORMAL TO THE STREAM

The applicability of inviscid-flow models to non-cavitating or cavitating flow past a normal plate is discussed. A new inviscid model is developed, with the aim of predicting features such as cavity length better than previous models. Experiments on air flow past a plate are described and the results compared with those of the theory. Finally the few experimental results available for cavitating flow are discussed.

A.R.C. C.P. No.697
November, 1962
Gadd, G. E. Ship Division, Nat. Phys. Lab.

TWO-DIMENSIONAL SEPARATED OR CAVITATING FLOW PAST A FLAT PLATE NORMAL TO THE STREAM

The applicability of inviscid-flow models to non-cavitating or cavitating flow past a normal plate is discussed. A new inviscid model is developed, with the aim of predicting features such as cavity length better than previous models. Experiments on air flow past a plate are described and the results compared with those of the theory. Finally the few experimental results available for cavitating flow are discussed.

A.R.C. C.P. No.697
November, 1962
Gadd, G. E. Ship Division, Nat. Phys. Lab.

TWO-DIMENSIONAL SEPARATED OR CAVITATING FLOW PAST A FLAT PLATE NORMAL TO THE STREAM

The applicability of inviscid-flow models to non-cavitating or cavitating flow past a normal plate is discussed. A new inviscid model is developed, with the aim of predicting features such as cavity length better than previous models. Experiments on air flow past a plate are described and the results compared with those of the theory. Finally the few experimental results available for cavitating flow are discussed.

Printed and published by
HER MAJESTY'S STATIONERY OFFICE
To be purchased from
York House, Kingsway, London W C 2
423 Oxford Street, London W.1
13A Castle Street, Edinburgh 2
109 St Mary Street, Cardiff
39 King Street, Manchester 2
50 Fairfax Street, Bristol 1
35 Smallbrook, Ringway, Birmingham 5
80 Chichester Street, Belfast 1
or through any bookseller

Printed in England

S O Code No. 23-9013-97

C.P. No. 697